Spring-like behavior of cementitious composite enabled by auxetic hyperelastic frame

Xu, Yading; Meng, Zhaozheng; Bol, Rowin J.M.; Šavija, Branko

DOI
10.1016/j.ijmecsci.2024.109364

Publication date
2024

Document Version
Final published version

Published in
International Journal of Mechanical Sciences

International Journal of Mechanical Sciences 275 (2024) 109364

Contents lists available at ScienceDirect

International Journal of Mechanical Sciences

journal homepage: www.elsevier.com/locate/ijmecsci

Spring-like behavior of cementitious composite enabled by auxetic hyperelastic frame

Yading Xu *, Zhaozheng Meng, Rowin J.M. Bol, Branko Šavija

Microlab, Delft University of Technology, the Netherlands

ARTICLE INFO

Keywords:
Mechanical properties
3D printing
Auxetic structures
Cementitious composites
Cyclic loading
Energy absorption

ABSTRACT

A novel highly compressible auxetic cementitious composite (ACC) is developed in this work. Contrary to conventional cementitious materials, such as plain concrete and fiber reinforced concrete, the ACC shows strain-hardening behavior under uniaxial compression: the stress continuously increases with strain up to approximately 40 % strain. On one hand, in the early compression stage, the ACC exhibit highly recoverable deformability of 10 % strain under cyclic loading (20 times higher than the constituent cementitious material). In addition, the ACC shows fatigue damage until the stiffness/strength and energy dissipation plateau values are reached after 500 cycles. At 2.5 % strain amplitude, the plateau stiffness/strength is approximately 120 MPa/3 MPa, while these values are only 25 MPa/1.2 MPa at 5 % strain amplitude. In contrast, the energy dissipation plateau of the ACC is independent from the amplitude and remains at 0.05 J/cm3. On the other hand, due to the strain-hardening behavior, the ACC exhibits significantly improved energy dissipation capacity compared to both the conventional cementitious materials and the auxetic frame. This behavior is achieved by a tailored composite action: integrating cementitious mortar with 3D printed thermoplastic polyurethane (TPU) auxetic frame. A rotating-square auxetic mechanism was designed for the TPU frame for the ACC to achieve the tailored cracking behavior. The horizontal ACC cells enable large deformability by enlarging the crack width under the confinement of the auxetic frame, while the vertical cells work as stiffening phase to ensure load resistance. Owing to the outstanding mechanical properties, the ACC shows great potential to be applied in engineering practice where high compressive deformability is required, for instance yielding elements for squeezing tunnel linings.

1. Introduction

Composites are commonly designed for materials to achieve enhanced mechanical properties. By properly designing the composite behavior, the property drawbacks of the constituent phases could be compensated or even enhanced such that the composite exhibits improved properties. In the field of civil engineering, cementitious materials are the most used construction materials [1,2]. The high compressive strength, high modulus and low cost ensured the application of cementitious materials in various engineering purposes. However, for long, plain cementitious materials have been criticized for the lack of ductility [1], which means that they are extremely prone to cracking under minor deformation. Therefore, in research and engineering practice, reinforced cementitious composites are usually used as an alternate for plain cementitious materials. For example, fibers have been used to improve the ductility of plain cementitious materials [3–5]. Through tailoring the composite action of the fibers and cementitious materials [6,7], even strain-hardening behavior under tensile load [7–9] can be achieved, although the cementitious matrix itself is quasi-brittle. In addition to creating fiber-reinforced composites, introducing architected cellular structures [10–12] has also been used to enhance ductility of plain cementitious mortar. For example, compressive strain-hardening behavior was achieved by introducing 2D [13–15] and 3D [16] auxetic structures.

In recent years, there has been a rapid development of 3D printing technology. 3D printed polymeric frames with various types of structures, for example triangular lattices [17], minimal surfaces [10,18], octet structures [19,20] have been used to significantly improve the ductility of cementitious materials. In these studies, polylactic acid (PLA) and acrylonitrile butadiene styrene (ABS) are commonly used as the reinforcement material. According to these studies, the stretchability of the polymeric materials is critical for the cementitious composites to achieve high ductility. The strain at break of the used PLA and ABS is normally 5 % to 10%, which is relatively low in the class of polymeric

* Corresponding author.
E-mail address: y.xu-5@tudelft.nl (Y. Xu).

https://doi.org/10.1016/j.ijmecsci.2024.109364
Received 7 February 2024; Received in revised form 25 April 2024; Accepted 3 May 2024
Available online 6 May 2024

materials. Several studies have found that lattice structures incorporating highly stretchable polymers (for instance thermoplastic polyurethane) could achieve better energy absorption [21], higher deformability [22], and cyclic loading resistance [23] than the lattice made of less stretchable polymer (such as e.g., PLA). This may indicate the possibility of applying such highly stretchable polymers to further improve the ductility of cementitious composites.

In contrast to aforementioned lattice structures, auxetic structures have a fascinating mechanical behavior: negative Poisson's ratio [13,24,25]. This means that auxetic structures exhibit lateral contraction under vertical compressive load, or lateral expansion under vertical tensile loaded [26–28]. The special mechanical response of auxetic structures allows for great deformability [29,30] and energy absorption ability [31–33]. Auxetic behavior is usually achieved by adopting periodic cells. This indicates that the shape or geometry of the cell structure crucially dominates the global mechanical performance of auxetic structures. Auxetic behavior are usually achieved by introducing structures with bending or rotation dominated mechanism [33–35], for example the typical re-entrant structure and its numerous analogous designs [29,36–40]. Such structures normally show lower stiffness than other non-auxetic lattice structures, which inhibits their application for load-bearing purposes. One possible approach to improve the stiffness of auxetic structures is optimizing the cell geometry [41,42], by locally adding extra component [38,41,43–45] or partially replacing the original unit cells [46–49] that have been actively studied in the past years.

Another potential approach is to infill [50,51] the auxetic structure and create composite materials. As a widely used engineering material, cementitious materials could be a potential choice of such filler. One of our previous study [52] already shows that using auxetics combined with cementitious materials to create a composite significantly improves the stiffness of the sole auxetic structures, and therefore achieved high compressive ductility of the composite. Some other studies have also indicated similar finding. For instance, it was found by [53] that when metal auxetic sheets are filled with foam concrete, the composite shows high ductility under static compression. A similar approach was applied by [54], while the composite was subjected to dynamic impact load, and it shows that the total energy absorption significantly increased with loading rate. Besides axial loading, research [55] has also shown that using polymeric auxetic fabrics at the bottom of a concrete beam, the energy absorption under flexural loading is also considerably enhanced.

For conventional cementitious materials, while the ductility in tension is more often investigated and discussed in research, in engineering practice, high compressive ductility and deformability can be also critical. A good example would be the yielding elements for tunnel linings [56]. In the construction of squeezing tunnels, the concrete (usually shotcrete) linings are potentially exposed to compressive pressure due to displacement of surrounding rocks. Therefore, steel yielding elements are often used to provide high compressive deformation capacity. A previous study [56] indicated that concrete reinforced by lattice structures can provide high compressive deformation capacity, and be used as an alternate of traditional steel yielding element. Similarly, our previous works have found that auxetic structure can significantly increase compressive deformability [16,52] of cementitious materials.

It is well known that auxetic structures exhibit horizonal contraction when subjected to uniaxial compressive load. Therefore, we have a hypothesis that this lateral contraction may be applied to confine crack initiation and propagation in cementitious materials under compressive loadings. Our previous work [52] has already shown the feasibility of such confinement by using 3D printing polymeric auxetic structures. In this study, we target even higher compressibility and energy absorption capacity, by further adopting a polymer with strikingly higher elasticity as the auxetic frame, such that a highly damage-resistant auxetic-cementitious composite (ACC) can be achieved. The composite is constituted by integrating the hard phase, i.e., a conventional plain cementitious mortar, and a soft phase, i.e., auxetic frame made of highly stretchable hyperelastic polymer. Specifically, the compressive behavior of the ACC is investigated both under uniaxial compression and cyclic loading. Moreover, the mechanism of the ACC composite action is clarified. The obtained results would inspire the great potential of integrating soft auxetic phases with cementitious materials to achieve highly ductile cementitious composites.

2. Materials and methods

2.1. Design and fabrication of the auxetic frame

The schematics of the designed auxetic frame is shown in Fig. 1. A planar shape with the so-called "rotating-square" [57] auxetic mechanism is adopted in this work. As seen in Fig. 1a, the struts of the used auxetic structure are derived from the virtual squares which are represented by the dashed line. The dimension of a unit cell of the designed auxetic structure is shown in Fig. 1b. The auxetic frame is generated by multiplating the unit cells, and extruded in the out-of-planed direction the thickness of 20 mm and 10 mm, respectively to form two series of ACC with different thickness. A commercial 3D printer Ultimaker 2+, was used to fabricate the auxetic frame. A hyperelastic thermoplastic polyurethane (TPU 95a from Ultimaker) was used as the printing material. The printing parameters of the auxetic frame are listed in Table 1. In addition, using the same printing parameters, dog-bone shape specimens (see Fig. 2) were also printed to study the mechanical properties of the 3D printed TPU material.

2.2. Mixing, casting, and curing

Considering the complex structure of the auxetic frame, a fine sand cementitious mortar with water-to-binder ratio of 0.4 was used. The cementitious mixture proportion is listed in Table 2.

Weighted dry materials (cement, fly ash and sand) were first mixed for 4 min. Then, water and superplasticizer were added, followed by another 4 min of mixing. Subsequently, the fresh mixture was casted in Styrofoam molds, in which the auxetic frames were glued before casting. Afterwards, the casted specimens were sealed and kept at room temperature. Two days after casting, the specimens were demolded and stored in a curing room (20 ± 2 °C, 96 ± 2 % RH) until the age of 28 days.

Before testing, the reference plain mortar (REF) and ACC specimens with two different thickness (T20 and T10) were cut to the designed

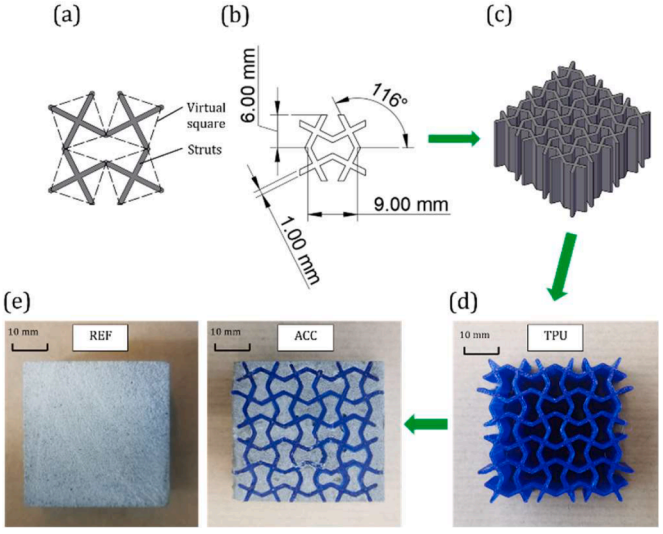

Fig. 1. (a) Schematics of the concept of "rotating-square" [57] auxetic structure; (b) an unit cell of the designed auxetic frame; (c) the designed auxetic frame for ACC; (d) 3D printed TPU frame; (e) casted ACC and reference specimen.

Table 1
Printing parameters.

Parameters	Configuration
Nozzle diameter (mm)	0.6
Temperature (°C)	235
Layer height (mm)	0.15
Line width (mm)	0.53
Infill density (%)	100
Printing speed (mm/s)	40

shape (length × width × thickness): 40 × 40 × 20 mm, denoted as T20; and 40 × 40 × 10 mm, denoted as T10. All prepared specimens are listed in Table 3. Several T20 specimens were painted in white background with black dots for digital image correction (DIC) analysis. The prepared TPU, ACC and reference specimens are shown in Fig. 1d and Fig. 1e, respectively.

2.3. Mechanical tests

Uniaxial tension tests were performed on the dog-bone shape specimens (shown in Fig. 2a), to understand the mechanical properties of the TPU material. The tests were conducted by the micro compression-tension test stage as shown in Fig. 2b, using displacement control at a constant load rate of 0.01 mm/s. The uniaxial compression tests were performed on the cured specimens by a hydraulic press INSTRON 8872 under displacement control at constant loading rate of 0.01 mm/s. During the tests, displacement and load were recorded by the INSTRON 8872. The experimental set-up is shown in Fig. 3a. Compressive load was applied on the specimen by two metal loading plates, and a piece of plastic film was placed between each loading plate and the specimen to reduce friction. A digital camera was placed in front of the specimen to take pictures of the tests. Cyclic loading tests were also performed by the same machine on the 20 mm thickness specimens (T20 and TPU). As shown in Fig. 3b and c, before the cyclic loading starts, the ACC specimens were first compressed to the equilibrium position at constant load rate of 0.01 mm/s. To study the impact of different cyclic amplitude on the mechanical performance of the ACC, two amplitudes, i.e., 1 mm (2.5 % strain) and 2 mm (5.0 % strain), were tested at the same frequency of 1 Hz.

2.3.1. Numerical modelling

To better understand the composite behavior of the ACC, especially the stress distribution under compressive load, a commercial numerical model package Abaqus was used to simply simulate the elastic response of the ACC under uniaxial compressive load. Corresponding to the planar design of the specimen, a two-dimensional model was generated. Triangular type mesh (CPS3) with an average size of 0.5 mm was used for the entire specimen. Compressive load was applied on the specimen by two rigid loading plates. To simulate the low friction boundary condition in the experiment and ensure no unrealistic horizontal sliding in the simulations, a minor friction coefficient 0.05 was assigned between the loading plates and the specimen. As the simulation only targets the elastic response, it is assumed that no interfacial sliding occurs

Table 2
Mixture design of the matrix material (kg/m^3).

CEM I 42.5 N	Fly ash	Sand (0.125~0.250 mm)	Superplasticizer (Glenium 51)	Water
473	559	473	2	413

Table 3
Prepared specimens.

Specimen	Dimension (length × width × thickness) [mm]
REF	40 × 40 × 20
T20	40 × 40 × 20
T10	40 × 40 × 10
TPU	40 × 40 × 20

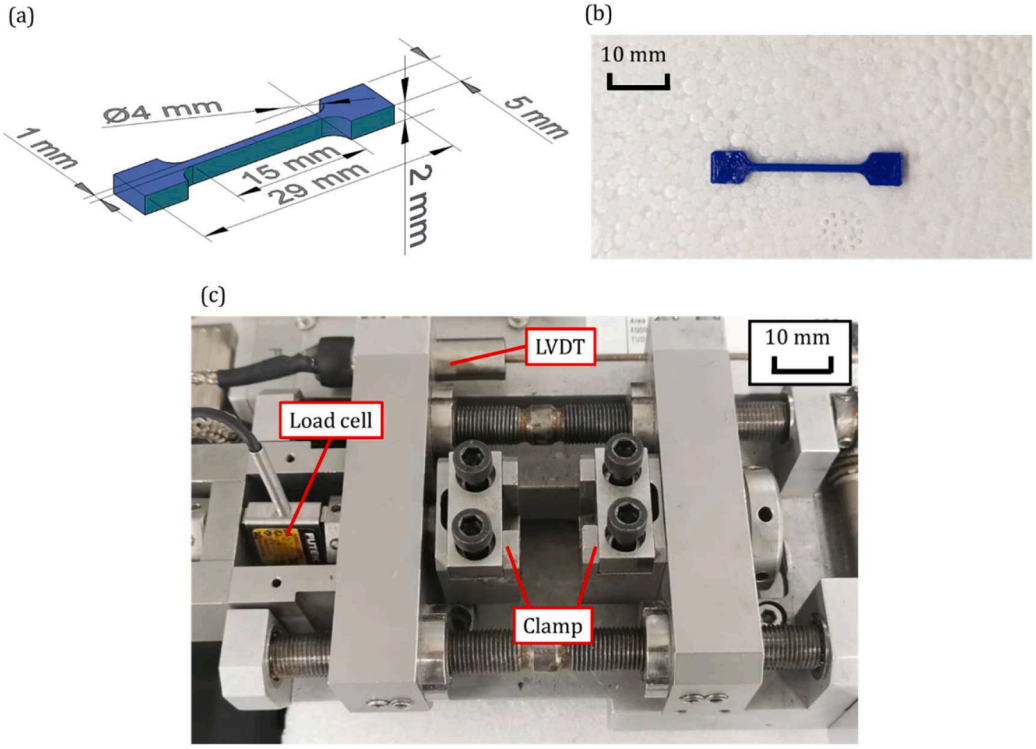

Fig. 2. (a) Schematics of the designed dog-bone shape specimen for understanding the constituent properties of the TPU material; (b) the 3D printed dog-bone specimen; (c) micro compression-tension test machine used for the mechanical tests of the TPU dog-bones.

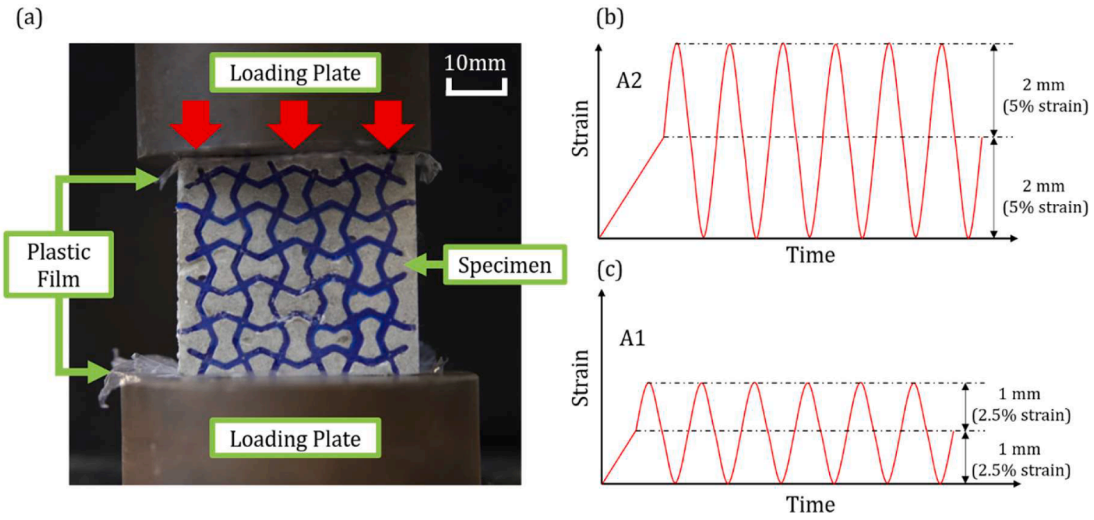

Fig. 3. (a) Experiment set-up of the compressive tests, uniaxial compressive load was applied on the ACC specimen by top loading plate while the bottom loading plate stayed still during the tests; (b) schematics of the cyclic loading at 2 mm/5 % strain amplitude, denoted as A2; (c) schematics of the cyclic loading at 1 mm/2.5 % strain amplitude, denoted as A1.

between the cementitious mortar and the TPU. After elastic stage, debonding may occur and influences the mechanical response of the ACC, however, it is beyond the target of the simulation here. In this sense, the "tie" interaction was used for the cementitious mortar and the TPU frame. The elastic modulus of TPU and cementitious mortar were obtained from previously described experiments and set as 85 MPa and 8821 MPa, respectively.

3. Results and discussions

3.1. Uniaxial compressive behavior

3.1.1. Deformation and stress-strain response

Prior to investigating the mechanical performance of the ACC, it is worth to first recall the compressive stress-strain response of conventional cementitious materials. The stress-strain curves of plain concrete and fiber reinforced concrete, consists two characteristic branches (depicted in Fig. 4) [1,2]: ascending branch and descending branch. In the ascending branch, stress increases with strain until the peak load (compressive strength) is reached. Within this branch, microcracking initiates in the compressed material, and subsequently propagates to form the main cracking planes. As a results, the stress decreases with strain forming a descending branch. Such compressive response is also termed as strain-softening behavior. In contrast to conventional cementitious materials, the ACC in this study exhibit strain-hardening behavior under uniaxial compressive load, namely the stress increases with strain as depicted in Fig. 4. Such strain-hardening behavior was previously achieved by cementitious cellular composites [13–16], while the ACC in this work have shown even better mechanical properties. This will be clarified in Section 3.1.2.

According to the experimental results shown in Fig. 5a, after initial micro cracking (witnessed by the several steep stress drops at approximately 2.5 % to 5% strain) the stress monotonically increases with strain. Note that, though the strain was only tested until approximately 40 % in the experiment, it was further increasing at this point. The compressive stress-strain response after this strain is normally termed as the "densification" stage [32], which is generated by crushing material residuals. Although the precise strain value where densification stage starts varies in different materials, it can be expected that the stress would rapidly increase with strain for the ACC at this stage. Similar results have been clarified in many other studies, for both auxetic materials [46,59–61] and conventional cementitious materials [1,56,62,63]. In addition, it is worth to be noticed is that the used auxetic frame is a 2D planar structure, the thickness of the ACC specimen may have an impact on the samples' mechanical behavior under compressive loading. As shown in Fig. 5b, for ACC with the thickness of 10 mm (T10), the

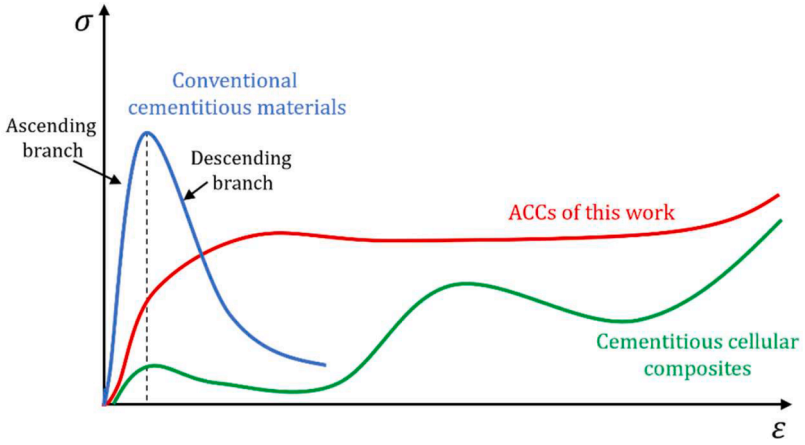

Fig. 4. Schematic of typical uniaxial compressive stress-strain response of conventional cementitious materials, cementitious cellular composites [13–16,58] and ACC of this work.

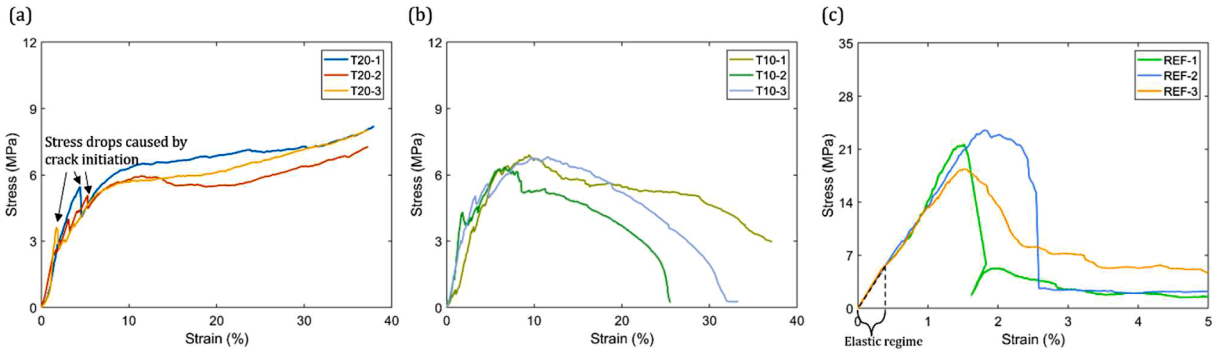

Fig. 5. Stress-strain curves of the under uniaxial compression, results from three duplicate specimens are shown, (a) ACC with 20 mm thickness (T20) shows monotonic strain-hardening behavior, namely stress continously increases with strain; (b) ACC with 10 mm thickness (T10) shows strain-softening behavior, namley stress decreases after peak load; (c) referecne cementitious mortar, note that the X-axis and Y-axis differ from the (a) and (b).

stress starts to drop after one peak load is reached (at approximately 10% strain). This was mainly caused by the buckling failure of the auxetic frame in the ACC, and it may significantly influence the energy absorption ability of the ACC. This point will be discussed in detail in Section 3.1.2. In sharp comparison to the ACC, the reference cementitious mortar (REF) in this work shows comparatively more brittle damage behavior and also exhibits the typical compressive strain-softening response, as shown in Fig. 5c.

Apart from the stress-strain response, the deformation and cracking mode of the new ACC is also distinct from conventional cementitious materials. As can be seen from Fig. 6a, at 5 % of strain, multiple distributed vertical cracks can be found on initiated on the compressed T20 specimen. However, these cracks did not propagate through the entire specimen. Even at 20 % strain, no main cracking plane appeared and, therefore, the ACC did not exhibit an obvious global failure and the stress could continuously increase. In addition to the sharp stress drops on the stress-strain curves (as seen in Fig. 5a), the DIC results present a more direct indication of the characteristic cracking behavior of the ACC. Corresponding to the multiple cracks found in Fig. 6, multiple localized high strain regions are present on the DIC results (as seen in Fig. 6b). Interestingly, the cracks in the ACC only initiated at the horizontal cells (the horizontal and vertical cells are differentiated in Fig. 6c), while the cementitious mortar in the vertical cells do not show any visible damage. As the strain increases to 5 % strain, enlargement of the crack width can be identified by the increased localized strain. This special cracking behavior allows the ACC to show the so-called spring-

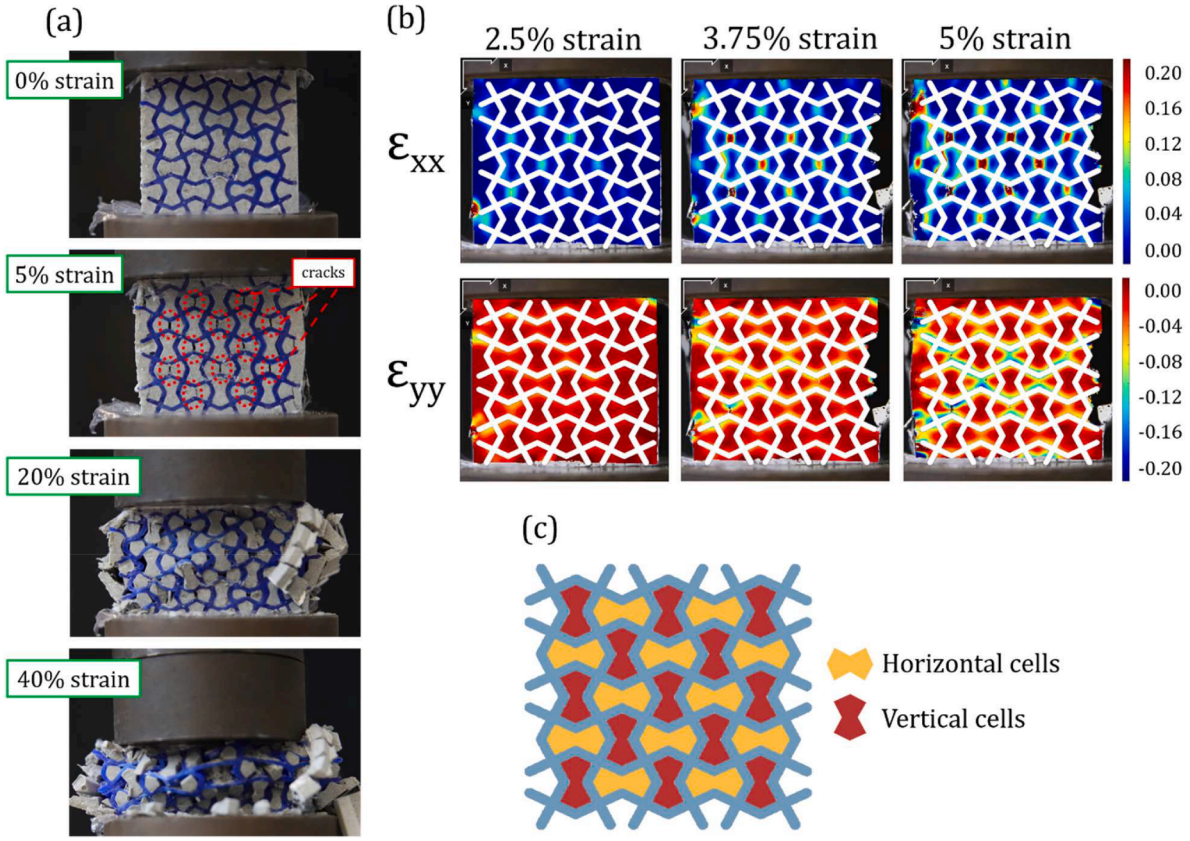

Fig. 6. (a) Deformation and damage mode of the ACC (T20) under uniaxial compression at different strain, (b) DIC results of the ACC at 5 % of strain, note that the position of the auxetic frame is marked in white, the legend indicated local strain; (c) schematics of horizontal and vertical cells, note that the outer most layer of cementitious mortar is not depicted.

like behavior under cyclic compressive loading, which will be further discussed in the Section 3.2.

The 3D printed auxetic TPU frame plays a crucial role in determining the unique compressive strain-hardening behavior of the ACC. This can be further verified by examining the compressive behavior of the auxetic frame itself. As seen in Fig. 7, the TPU frame by itself also exhibits strain-hardening compressive behavior, although the compressive stress is significantly lower than the ACC. More importantly, the TPU frame shows auxetic deformation mode, which contributes to confine the enlargement of the initiated cracks in the horizontal cells of the ACC as seen in Fig. 7a. In the meanwhile, the highly deformable nature of the TPU materials is a crucial factor for the auxetic frame to resist such high deformation. As can be seen from Fig. 7b, the TPU material shows great stretchability without obvious failure until 40 % strain. Similar highly stretchable behavior of hyperelastic material is also seen in other studies [64–66].

3.1.2. *Energy absorption ability*

An advantage of possessing strain-hardening behavior is that the ACC show outstanding energy absorption ability (defined as the area below load-displacement curve per volume) in compression. Recently, besides the ACC created in this work, compressive strain-hardening behavior was also achieved by creating tailored auxetic cellular structures, as reported in [13–16]. As shown in Fig. 8a, compared to the conventional cementitious mortar and the TPU frame, the energy absorption of the ACC with different thickness (T20 and T10) and cellular composites reported in [13–16] is strikingly higher: the ACC (T20) achieved 4200 % higher than the cementitious mortar with the same mixture, and 6300 % higher than the TPU auxetic frame. Furthermore, the ACC shows 88 % higher energy absorption than the cementitious cellular composites reported in [13–16], which also shows great energy absorption properties.

Moreover, because of the damage process of the cellular structure under compression, the composites in [13–16] exhibits considerable stress decrease (as indicated in Fig. 4) before the strain-hardening initiated. In sharp contrast, as the ACC in this work do not have a cellular geometry, the stress could monotonically increase with strain. As a result, it can be seen from the Fig. 8a that total absorbed energy of the ACC (T20) under uniaxial compression is approximately two times higher than the cellular composites with auxetic behavior (Cellular).

As already indicated by the stress-strain curves of T20 and T10 in Fig. 5a and b. the thickness of the ACC specimen shows obvious impact on the samples' energy absorption ability under compressive loading. This was mainly caused by the buckling failure of the auxetic frame in the ACC. As can be seen from Fig. 8b, out-of-plane buckling appeared after the T10 ACC was compressed while such deformation was not observed on the T20 specimens. As a result, the overall energy absorption of the T10 ACC is considerably lower than that of T20 as indicated

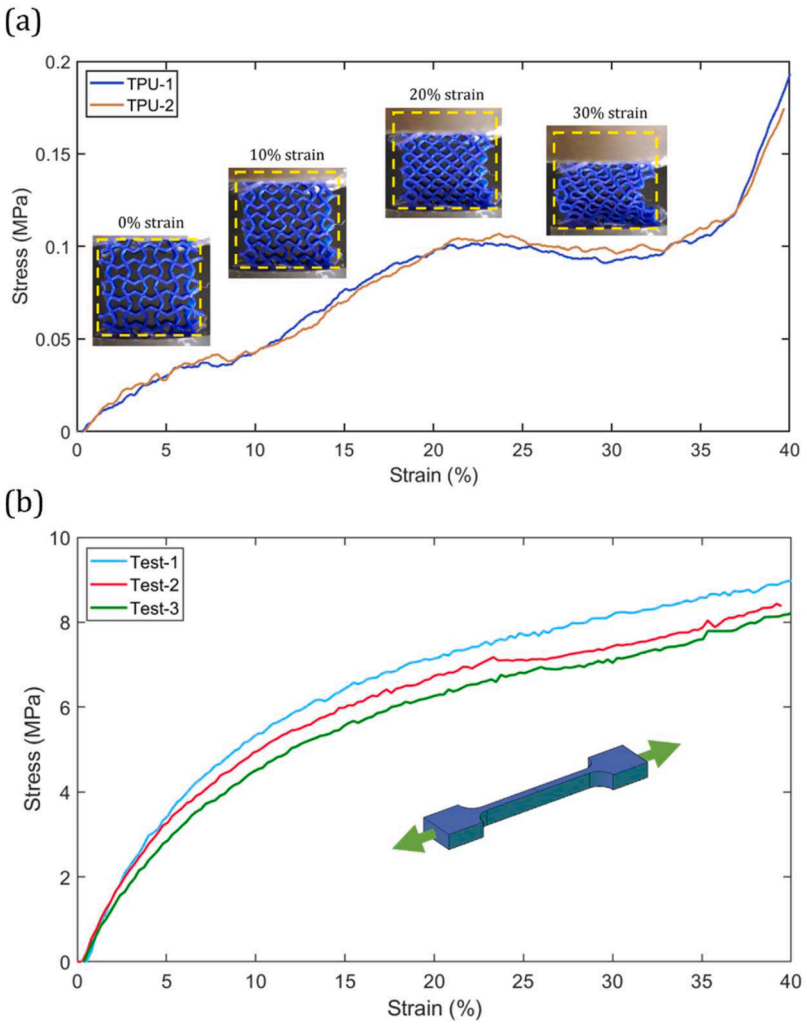

Fig. 7. (a) Stress-strain curves of the 3D printed TPU auxetic frame, results from two duplicates are shown; (b) Uniaxial tensile response of the 3D printed TPU material, note that the experiment only tested until 40 % strain to compare with the compressive behavior of ACC, the actual elongation at break of the TPU is 560% strain according to the manufacturer [67].

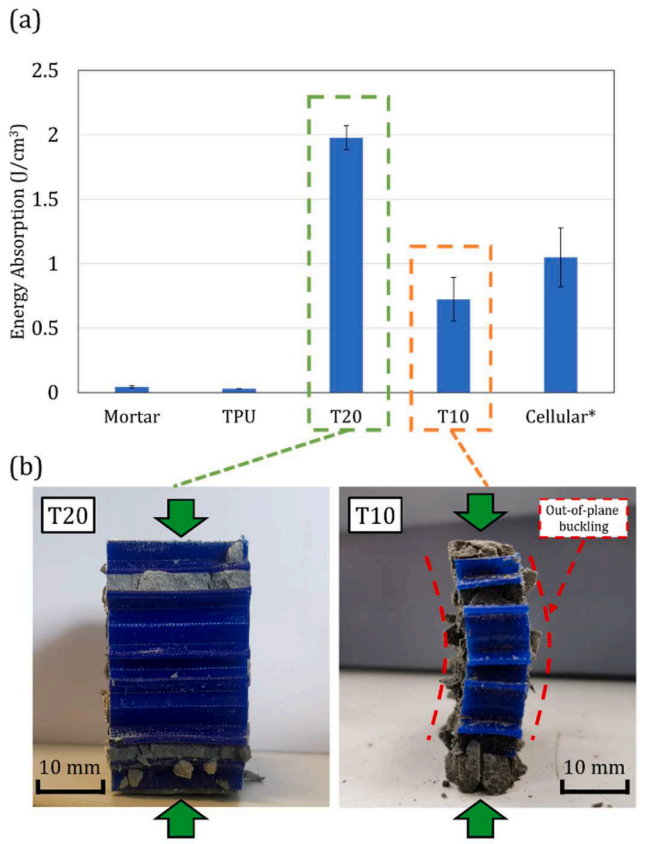

Fig. 8. (a) Comparison of the energy absorption of the ACC and other materials under uniaxial compression; *the data of the cementitious cellular composites is adopted from [13–16], standard deviation is indicated; (b) out-of-plane buckling failure is only witnessed on the specimens with 10 mm (T10) thickness after compression.

in Fig. 8a.

For the strain-hardening behavior of the ACC, there could be a very specific engineering application: yielding elements/yielding supports [68] for squeezing tunnel linings. It was mentioned by [56], concrete reinforced with lattice structure shows high compressibility, therefore, may be used as yielding elements for deep tunnel linings which are usually exposed to pressure induced by surrounding rocks. The yielding elements are commonly used as joints between tunnel lining segments to allow large deformation and maintain pressure level in the linings. The strain-hardening compressive response of the ACC highly satisfies the target stress-strain response as elaborated by [68,69] of such yielding elements. Comparing to conventional steel yielding elements, such ACC may help to solve the corrosion problem in underground environment, while the construction cost of the ACC may still be much higher as 3D printing techniques is required to produce a large number of such elements.

3.2. Spring-like behavior under cyclic loading

3.2.1. Hysteresis stress-strain response

As discussed in the previous section, the ACC's have shown outstanding energy absorption ability, under uniaxial compression. More importantly, the ACC's also exhibit the so-called "spring-like" behavior. This means that the, as cementitious material, the ACC's show highly recoverable deformability under cyclic loading similar to the behavior of a spring (see Fig. 9). The choice of cyclic loading amplitude is based on the uniaxial compressive stress-strain curves (Fig. 5a) of the ACC. We found that at approximately 10% of strain, a "peak" compressive stress is reached and afterwards stress stays relatively

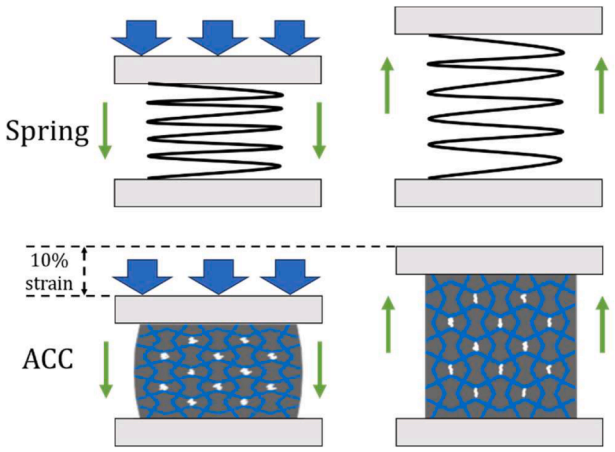

Fig. 9. Schematics of the deformation mode of ACC and a spring under certain pressure, both exhibit recoverable deformation, for the ACC in this work at least 10% of cyclic strain is reached, compared to conventional cementitious mortar 10 % deformability is significantly higher.

stable until 40 % of strain. This implies that even increase the amplitude range to significantly more than 10% strain, the stress would not show obvious change. Therefore, before 10 % is the most interesting range where the specimen may sharply indicate the damage behavior. In addition, at approximately 5% strain cracks start to appear (indicate by the stress drops) and at approximately. So, it could be also interest to investigate the cracking behavior within a range where the cracks are just started to initiate.

As can be seen from Fig. 10, the stress-strain curves of the ACC present typical hysteresis responses under cyclic loading. In each cycle (as seen in Fig. 10c), a loading and unloading branch can be identified: in the loading branch, the stress increases with strain; when the strain reaches the prescribed amplitude, a peak stress is reached (herein, the peak stress is defined as the strength of the ACC within this cycle); afterwards, the stress decreases with strain such that an un-loading branch is formed, and one cycle is completed. For conventional cementitious materials, for instance the plain cementitious mortar used in this work, deformation is only recoverable in the elastic regime (defined as the branch before 30 % of the compressive strength as indicated in Fig. 5c) which is only 0.53 (±0.07)%. In this sense, under 2 mm (5 % strain) amplitude the ACC achieved approximately 20 times higher recoverable deformation compared to the conventional cementitious mortar. Similar behavior was also found on the cementitious cellular composites [13–16], while the plateau strength of them is only 0.2 MPa, which is considerably lower than the ACC in this work.

It is clearly seen in Fig. 10a and b that the compressive strength of the ACC reduces as the number of cycles increases. Especially, at the beginning of the cyclic tests, the strength decreases rapidly with the cycle numbers. Such strength reduction indicates the rigidity loss of the ACC due to fatigue damage, which is commonly seen in polymeric auxetics [70,71], metallic auxetics [72,73] and cementitious auxetic composites [14]. This can be quantified by the stiffness (as defined in Fig. 10c) degradation of the ACC. The stiffness degradation from the initial cycles is significant. However, as the number of cycles increase a plateau was eventually reached (see Fig. 11a). Although in the long term after 500 cycles, the stiffness may continue to decrease. It is expected that such stiffness decrease may appear at a very low rate similar to what we have found on the cellular composites in our previous study [14], therefore, not presented here in this work. However, the long-term fatigue behavior of the ACC is worth of studying as it may provide knowledge on the competence of the ACC for potential engineering applications with damping and vibration isolation requirements, similar to solely using auxetic structures [74,75].

It is worth mentioning that the plateau stiffness of the ACC is not

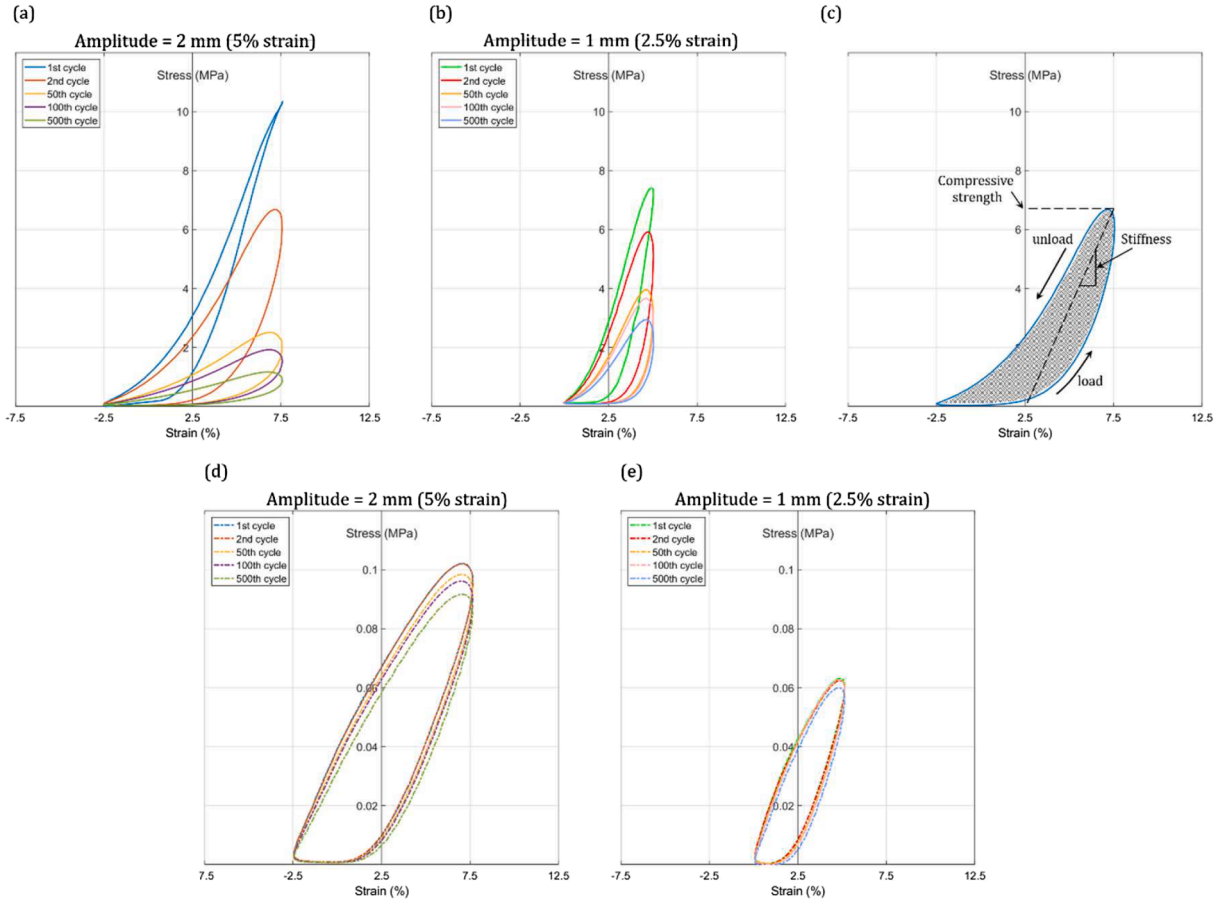

Fig. 10. Stress-strain curves of the (a) ACC under 2 mm amplitude cyclic loading, (b) ACC under 1 mm amplitude cyclic loading; (c) a typical stress-strain curve within one single cycle; (d) TPU under 2 mm amplitude cyclic loading; (e) TPU under 1 mm amplitude cyclic loading, that all curves are centered by their equilibrium strain positions.

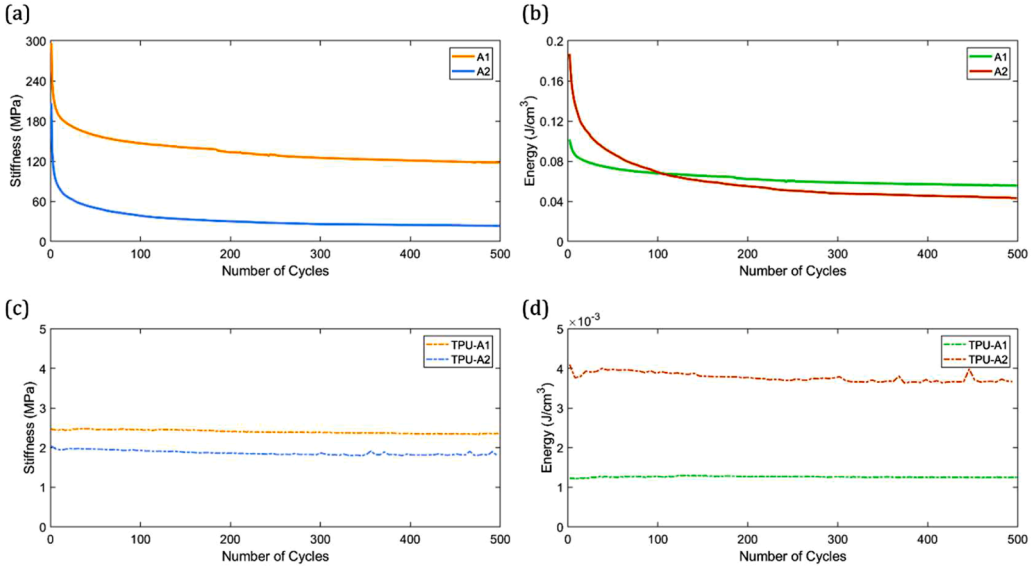

Fig. 11. (a) Stiffness degradation of the ACC; (b) energy dissipation degradation of the ACC caused by fatigue damage under 1 mm (A1) and 2 mm (A2) amplitude in each cycle; (c) stiffness of TPU maintained stable under both amplitude (d) energy dissipation of TPU also almost maintained at certain levels under both amplitude.

simply an intrinsic property, but highly dependent on the amplitude of the imposed cyclic loading. As seen from Fig. 11a, under 1 mm amplitude (Fig. 11a A1), the plateau stiffness is approximately 120 MPa (3 MPa strength), while at 2 mm amplitude (Fig. 11a, A2) the value is only 25 MPa. The rapid loss of stiffness of A2 is attributed to potential higher internal fatigue damage introduce by the cyclic loadings. Larger

amplitude introduces more damage to the cementitious mortar, therefore, the plateau stiffness of A2 is obviously lower than A1. Furthermore, although the rigidity loss also indicates the reduction in energy dissipation in each cycle, according to Fig. 11b the amplitude shows minor impact on the plateau energy dissipation of the ACC. At 500 cycles, the energy dissipated in each cycle remains approximately 0.05 J/cm^3 under both amplitude values. Although the plateau energy dissipation is considerably lower than the energy absorbed under one uniaxial compression, the ability to withstand multiple cycles significantly improves the total energy absorption ability of the ACC.

The TPU frame also exhibits hysteretic stress-strain response under cyclic loading (Fig. 10d and e), accompanied by the typical auxetic deformation behavior (see Fig. 12b). However, at the same cyclic strain, the stress of the TPU is strikingly lower than that of the ACC in each cycle. The reason is that the stiffness and strength of the TPU frame is significantly lower than that of the ACC. As shown in Fig. 11c, the stiffness of TPU frame is 2.0 ~ 2.5 MPa, which is only 2 % of the plateau stiffness of the ACC (120 MPa). Therefore, the TPU frame is not able to provide such high rigidity for the ACC. In other words, the rigidity of the ACC mainly comes from the un-cracked cementitious mortar in the vertical cells. Furthermore, owing to the improved rigidity provided by the cementitious mortar, the energy dissipation of the ACC is also considerably higher compared to the TPU frame itself. As can be seen in Fig. 11d, the maximum plateau energy dissipation of the TPU frame is only 0.004 J/cm^3 in each cycle. This is only 10 % of the energy dissipation plateau value of the created ACC (approximately 0.04 J/cm^3).

3.2.2. *The tailored composite action*

The mechanism of the previously discussed spring-like behavior under cyclic loading is attributed to the tailored two-stage composite reaction of the ACC. The designed TPU frame and the cementitious mortar cells of the ACC play different roles which ensure such unique mechanical properties: the horizontal cells enable large deformability while the vertical cells ensure rigidity under cyclic loading. The first stage of the composite action is the oriented crack initiation: according to the numerical simulation results shown in Fig. 12a, when subject to compressive load, tensile stress mainly appears in the horizontal cells of the ACC. Due to the intrinsic brittleness of the cementitious mortar, cracks are expected to initiate at these regions. This agrees very well with our experimental findings: visible cracks were only found to be in these horizontal cells. After crack initiation, in the loading branch of each cycle, as strain increases the cracked horizontal cells allow the ACC to withstand large deformation, by enlarging the crack width (as seen in Figs. 6b and 12a) under the confinement of the highly deformable TPU frame. Afterwards, in the unloading branch of each cycle, as strain decreases the auxetic behavior of the TPU frame allows the ACC to recover deformation, thus consequently accompanied by the narrowing of these enlarged cracks (see Fig. 12b). It is worth mentioning that the ACC does not show negative Poisson's ratio under compression. This was mainly caused by the difference in stiffness of the TPU and cementitious mortar. The elastic modulus of cementitious mortar (8821 MPa) is significantly higher than that of TPU (85 MPa). A similar effect has also been reported in the literature [76].

What needs to be further mentioned is that, due to the hyperelastic nature of the TPU material the auxetic frame shows much less fatigue damage under cyclic loading compared to the ACC. This can be easily seen from Fig. 10, the stiffness/strength and energy absorption of the TPU from almost maintained constant with the number of cyclic loading increases. In this sense, it is inferred that the obvious fatigue damage of the ACC is mainly attributed to the cementitious mortar. As the number

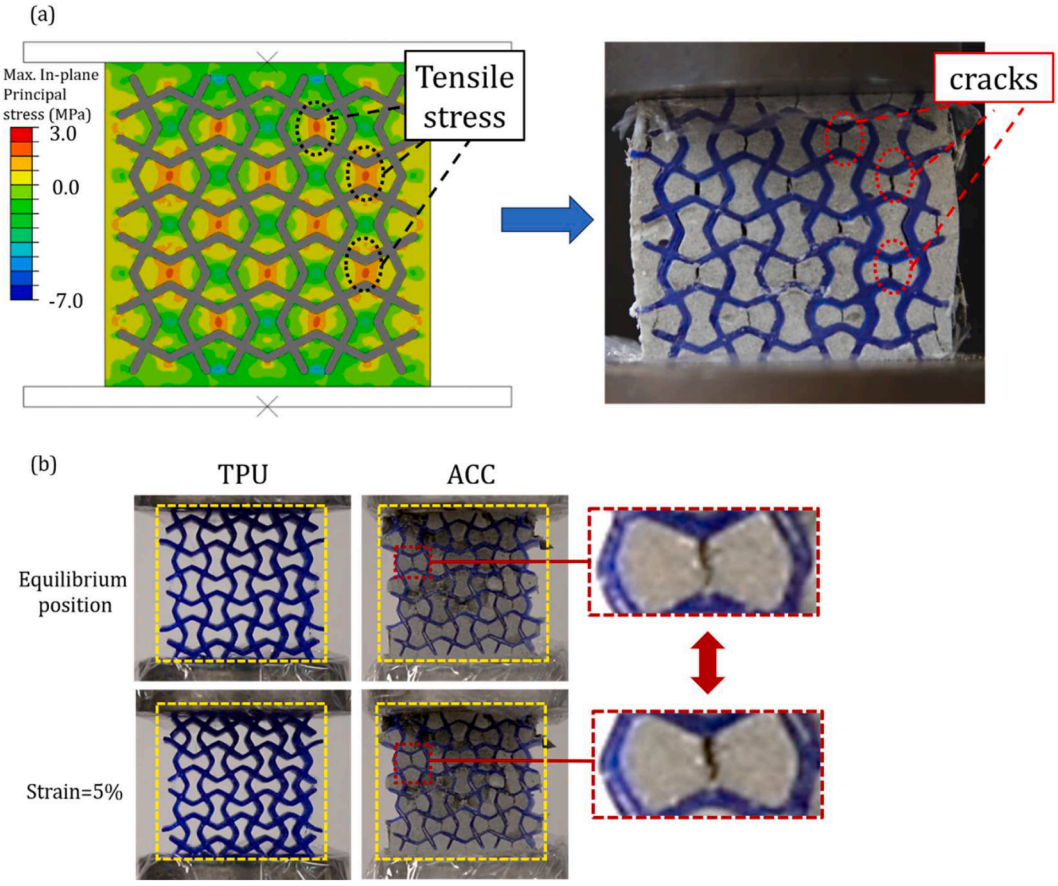

Fig. 12. (a) Simulated stress distribution in the cementitious mortar at the elastic stage, consequently crack initiates at locations with high principal (tensile) stress, it is clearly shown that high tensile stress locates only in the horizontal cells where cracks are expected.

of cycle increases, cracks may also appear in the vertical cells after certain number of cycles. As such, we can assume that instead of plain mortar, using fiber-reinforce cementitious materials (FRCs) as the filler in inside the auxetic structures may significantly enhance the fatigue resistance of the ACC. On one hand, the FRC itself already has good cracking resistance owing to the interaction between fiber and cementitious mortar. Therefore, it could considerably mitigate the stiffness/energy absorption degradation caused by crack formation and enlargement in cementitious mortar. On the other hand, the potential fibrillation phenomenon [77] of the fibers after cyclic loading may create excessive fiber branches in the cementitious matrix, thus even increase energy dissipation of the composites by introducing more friction within the cementitious material. Furthermore, in future studies in case the FRCs are used as the filling material, the fiber length has to be carefully considered when designing the auxetic frame, such that fibers can be properly distributed in the auxetic cells.

4. Conclusions

This work presents a study on the mechanical behavior of a novel auxetic cementitious composite (ACC) exhibiting spring-like compressive behavior. The composite is developed by a compositing strategy: using 3D printed thermoplastic polyurethane (TPU) auxetic structure as deformable frame and the cementitious mortar as stiffening filler. Uniaxial compression and cyclic loading tests are performed to characterize the mechanical properties of the developed ACC. As a composite material, the ACC takes advantage of both constituent phases and achieves improved mechanical properties over the properties of the TPU and cementitious mortar. According to the obtained results, several conclusions can be drawn:

The ACC shows strikingly higher energy absorption ability, compared to the reference conventional cementitious mortar and the polymeric auxetic TPU frame. Due to the monotonic strain-hardening behavior under uniaxial compression, namely the stress continuously increases with strain, the ACC achieved 4200 % and 6300 % higher energy absorption ability compared to the reference mortar and the polymeric TPU frame, respectively.

Contrary to conventional cementitious materials, the ACC exhibits an out-standing spring-like compressive behavior. This behavior allows ACC with extremely high recoverable deformability under compressive cyclic loading. In this work, at least 5 % strain amplitude (10 % strain in total) was reached, which is approximately 20 times higher than the conventional reference cementitious mortar. The damage and deformation mechanism of such behavior is attributed to a two-stage tailored composite action of the ACC. The first stage is the oriented stress distribution and crack initiation: the auxetic frame induced tailored internal stress distribution such that cracks only initiate at preferred locations. The second stage is the confined crack width enlargement in cementitious mortar by the auxetic behavior of the hyperelastic TPU frame.

Although the ACC exhibits obvious fatigue damage under cyclic loading, it shows significantly improved stiffness and energy absorption than the auxetic frame. After 500 cycles, plateau stiffness and energy dissipation are reached by the ACC. The stiffness plateau achieved 120 MPa (50 times higher than auxetic frame) and 25 MPa (12 times higher than auxetic frame) under 2.5 % strain amplitude and 5 % strain amplitude, respectively. In comparison, the energy dissipation plateau in each cycle is found independent of the amplitude and maintains at approximately 0.04 J/cm^3 (10 times higher than auxetic frame).

Different from common engineering applications where high strength and stiffness is usually required for cementitious materials, in case of aforementioned concrete linings, high compressive deformability is needed to resist potential compressive pressure induced by surrounding rocks. The developed ACC in this work shows great recoverable compressive deformability and energy absorption ability which potentially makes the ACC an alternate for conventional yielding elements or yielding supports which requires high compressive deformability.

CRediT authorship contribution statement

Yading Xu: Writing – review & editing, Writing – original draft, Methodology, Investigation, Formal analysis, Data curation, Conceptualization. **Zhaozheng Meng:** Writing – review & editing. **Rowin J.M. Bol:** Writing – review & editing. **Branko Šavija:** Writing – review & editing, Project administration, Funding acquisition.

Declaration of competing interest

The authors declare that they have no known competing financial interests or personal relationships that could have appeared to influence the work reported in this paper.

Data availability

The data that support the findings of this study are available from the corresponding author Dr. Yading Xu, upon reasonable request.

Acknowledgements

The authors acknowledge the financial support from the European Research Council (ERC) within the framework of the ERC Starting Grant Project “Auxetic Cementitious Composites by 3D printing (ACC-3D)”, Grant Agreement Number 101041342. Views and opinions expressed are however those of the author(s) only and do not necessarily reflect those of the European Union or the European Research Council. Neither the European Union nor the granting authority can be held responsible for them.

References

[1] Van Mier JG. Fracture processes of concrete. CRC Press; 1997.
[2] Van Mier JG. Concrete fracture: a multiscale approach. CRC Press; 2012.
[3] Li VC, et al. On the emergence of 3D printable engineered, strain hardening cementitious composites (ECC/SHCC). Cem Concr Res 2020;132:106038.
[4] Savastano H, et al. Fracture and fatigue of natural fiber-reinforced cementitious composites. Cement Concrete Compos 2009;31(4):232–43.
[5] Ding T, et al. Anisotropic behavior in bending of 3D printed concrete reinforced with fibers. Compos Struct 2020:254.
[6] Li, V.C., et al., Interface tailoring for strain-hardening polyvinyl alcohol-engineered cementitious composite (PVA-ECC). 2002.
[7] Li, V.C., On engineered cementitious composites (ECC). 2003.
[8] Li, V.C., From micromechanics to structural engineering-the design of cementitous composites for civil engineering applications. 1993.
[9] Kanda T, Li VC. New micromechanics design theory for pseudostrain hardening cementitious. J Eng Mech 1999;125(4):373–81.
[10] Nguyen-Van V, et al. Dynamic responses of bioinspired plastic-reinforced cementitious beams. Cement Concrete Compos 2022;133:104682.
[11] Nguyen-Van V, et al. Digital design computing and modelling for 3-D concrete printing. Autom Constr 2021;123:103529.
[12] Nguyen-Van V, et al. Bioinspired cellular cementitious structures for prefabricated construction: hybrid design & performance evaluations. Autom Constr 2020;119:103324.
[13] Xu Y, Šavija B, Schlangen E. Compression behaviors of cementitious cellular composites with negative poisson’s ratio. in framcos. France; 2019.
[14] Xu Y, et al. Cementitious cellular composites with auxetic behavior. Cement Concrete Compos 2020;111:103624.
[15] Xu Y, et al. Tunable mechanical behavior of auxetic cementitious cellular composites (CCCs): experiments and simulations. Constr Build Mater 2021;266:121388.
[16] Xu Y, Šavija B. 3D auxetic cementitious-polymeric composite structure with compressive strain-hardening behavior. Eng Struct 2023;294:116734.
[17] Xu Y, Šavija B. Development of strain hardening cementitious composite (SHCC) reinforced with 3D printed polymeric reinforcement: mechanical properties. Compos Part B Eng 2019;174:107011.
[18] Nguyen-Van V, et al. Performance of concrete beam reinforced with 3D printed Bioinspired primitive scaffold subjected to three-point bending. Autom Constr 2022;134:104060.

[19] Xu Y, et al. Cementitious composites reinforced with 3D printed functionally graded polymeric lattice structures: experiments and modelling. Additive Manufacturing; 2021, 101887.
[20] Salazar B, et al. Polymer lattice-reinforcement for enhancing ductility of concrete. Mater Des 2020;196:109184.
[21] Yavas D, et al. Design and fabrication of architected multi-material lattices with tunable stiffness, strength, and energy absorption. Mater Des 2022:217.
[22] Mansouri MR, et al. 3D-printed multimaterial composites tailored for compliancy and strain recovery. Compos Struct 2018;184:11–7.
[23] Johnston R, Kazancı Z. Analysis of additively manufactured (3D printed) dual-material auxetic structures under compression. Addit Manuf 2021;38.
[24] Wu Y, et al. Additively manufactured materials and structures: a state-of-the-art review on their mechanical characteristics and energy absorption. Int J Mech Sci 2023;246:108102.
[25] Wang E, et al. Lightweight metallic cellular materials: a systematic review on mechanical characteristics and engineering applications. Int J Mech Sci 2024;270:108795.
[26] Gomes RA, et al. Tubular auxetic structures: a review. Thin-Walled Struct 2023;188:110850.
[27] Shukla S, Behera BK. Auxetic fibrous structures and their composites: a review. Compos Struct 2022;290:115530.
[28] Montgomery-Liljeroth E, Schievano S, Burriesci G. Elastic properties of 2D auxetic honeycomb structures- a review. Appl Mater Today 2023;30:101722.
[29] Jiang F, et al. Fabrication and crushing response of graded re-entrant circular auxetic honeycomb. Int J Mech Sci 2023;242:107999.
[30] da Silva LCM, Grillanda N, Casolo S. Heuristic molecular modelling of quasi-isotropic auxetic metamaterials under large deformations. Int J Mech Sci 2023;251:108316.
[31] Wu W, et al. Mechanical design and multifunctional applications of chiral mechanical metamaterials: a review. Mater Des 2019;180:107950.
[32] Zhang J, Lu G, You Z. Large deformation and energy absorption of additively manufactured auxetic materials and structures: a review. Compos Part B Eng 2020;201:108340.
[33] Zhou J, et al. Comparison of different quasi-static loading conditions of additively manufactured composite hexagonal and auxetic cellular structures. Int J Mech Sci 2023;244:108054.
[34] Li T, Liu F, Wang L. Enhancing indentation and impact resistance in auxetic composite materials. Compos Part B Eng 2020;198.
[35] Montazeri A, et al. Auxetic mechanical metamaterials with symmetry-broken Re-entrant units. Int J Mech Sci 2024;266:108917.
[36] Hu Q, Lu G, Tse KM. Compressive and tensile behaviours of 3D hybrid auxetic-honeycomb lattice structures. Int J Mech Sci 2024;263:108767.
[37] Yang L, et al. Mechanical properties of 3D re-entrant honeycomb auxetic structures realized via additive manufacturing. Int J Solids Struct 2015;69-70:475–90.
[38] Chen Z, et al. Re-entrant auxetic lattices with enhanced stiffness: a numerical study. Int J Mech Sci 2020;178:105619.
[39] Ma N, et al. Hierarchical re-entrant honeycomb metamaterial for energy absorption and vibration insulation. Int J Mech Sci 2023;250:108307.
[40] Montazeri A, Bahmanpour E, Safarabadi M. A Poisson's ratio sign-switching mechanical metamaterial with tunable stiffness. Int J Mech Sci 2023;260:108670.
[41] Zhu D, et al. A novel elliptical annular re-entrant auxetic honeycomb with enhanced stiffness. Int J Mech Sci 2024;262:108732.
[42] Yu S, et al. The compressive responses and failure behaviors of composite graded auxetic re-entrant honeycomb structure. Thin-Walled Struct 2023;187:110721.
[43] Chen Y, Fu MH. A novel three-dimensional auxetic lattice meta-material with enhanced stiffness. Smart Mater Struct 2017;26(10):105029.
[44] Fu MH, Chen Y, Hu LL. A novel auxetic honeycomb with enhanced in-plane stiffness and buckling strength. Compos Struct 2017;160:574–85.
[45] Jafari Nedoushan R, et al. Novel triangular auxetic honeycombs with enhanced stiffness. Compos Struct 2021;277:114605.
[46] Cheng X, et al. Design and mechanical characteristics of auxetic metamaterial with tunable stiffness. Int J Mech Sci 2022;223.
[47] Xu M, et al. Mechanical properties and energy absorption capability of AuxHex structure under in-plane compression: theoretical and experimental studies. Int J Mech Sci 2019;159:43–57.
[48] Qi C, et al. Multi-scale characterization of novel re-entrant circular auxetic honeycombs under quasi-static crushing. Thin-Walled Struct 2021;169:108314.
[49] Jeong S, Yoo HH. Shape optimization of bowtie-shaped auxetic structures using beam theory. Compos Struct 2019;224:111020.
[50] Acharya A, et al. An infill-based approach towards stiffer auxetic lattices: design and study of enhanced in-plane elastic properties. Mech Mater 2024;188:104849.
[51] Albertini F, et al. Experimental and computational analysis of the mechanical properties of composite auxetic lattice structures. Addit Manuf 2021;47:102351.
[52] Xu Y, Šavija B. Auxetic cementitious composites (ACCs) with excellent compressive ductility: experiments and modeling. Mater Des 2024:237.
[53] Zhong R, et al. Mechanical properties of concrete composites with auxetic single and layered honeycomb structures. Constr Build Mater 2022;322:126453.
[54] Borchers A, Pieler T. Programming pluripotent precursor cells derived from Xenopus embryos to generate specific tissues and organs. Genes 2023;1(3):413–26 (Basel).
[55] Asad M, et al. Enhanced energy absorption of auxetic cementitious composites with polyurethane foam layers for building protection application. J Build Eng 2023;78:107613.
[56] Salazar B, et al. Highly compressible concrete: the effect of reinforcement design on concrete's compressive behavior at high strains. Mater Des 2023;230.
[57] Grima JN, Evans KE. Auxetic behavior from rotating squares. J Mater Sci Lett 2000.
[58] Xie J, et al. Peanut shaped auxetic cementitious cellular composite (ACCC). Constr Build Mater 2024;419:135539.
[59] Zhao C, et al. Experimental study and finite element analysis on energy absorption of carbon fiber reinforced composite auxetic structures filled with aluminum foam. Compos Struct 2023;303.
[60] Zhang XG, et al. A novel auxetic chiral lattice composite: experimental and numerical study. Compos Struct 2022;282:115043.
[61] Choudhry NK, Panda B, Kumar S. In-plane energy absorption characteristics of a modified re-entrant auxetic structure fabricated via 3D printing. Compos Part B Eng 2022;228.
[62] Yang Y, Zhou Q, Deng Y. The reinforcement attributes of multi-scale hybrid fiber throughout the uniaxial compression of ultra-low-weight foamed cement-based composites. Constr Build Mater, 242; 2020, 118184.
[63] Alam A, Hu J. Mechanical properties and energy absorption capacity of plain and fiber-reinforced single- and multi-layer cellular concrete. Constr Build Mater, 394; 2023.
[64] Wang Y, et al. Simplification of hyperelastic constitutive model and finite element analysis of thermoplastic polyurethane elastomers. Macromol Theory Simul 2020;29(4).
[65] Hamzehei R, et al. Octagonal auxetic metamaterials with hyperelastic properties for large compressive deformation. Int J Mech Sci 2018;145:96–105.
[66] Rezaei S, et al. Design and modeling of the 2D auxetic metamaterials with hyperelastic properties using topology optimization approach. Photonics Nanostructures Fundam Appl 2021;43:100868.
[67] Ultimaker, Ultimaker TPU technical data sheet. 2022.
[68] Wu K, et al. A critical review on the performance of yielding supports in squeezing tunnels. Tunn Undergr Space Technol 2021;115:103815.
[69] Moritz B. Yielding elements – requirements, overview and comparison /Stauchelemente – Anforderungen, Überblick und Vergleich. Geomech Tunn 2011;4(3):221–36.
[70] Bezazi A, Scarpa F. Mechanical behaviour of conventional and negative Poisson's ratio thermoplastic polyurethane foams under compressive cyclic loading. Int J Fatigue 2007;29(5):922–30.
[71] Bouchahdane K, Ouelaa N, Belaadi A. Static and fatigue compression behaviour of conventional and auxetic open-cell foam. Mech Adv Mater Struct 2021;29(27):6154–67.
[72] Lvov VA, et al. Low-cycle fatigue behavior of 3D-printed metallic auxetic structure. Mater Today Proc 2020;33:1979–83.
[73] Kolken HMA, et al. Fatigue performance of auxetic meta-biomaterials. Acta Biomater 2021;126:511–23.
[74] Duc ND, et al. Dynamic response and vibration of composite double curved shallow shells with negative Poisson's ratio in auxetic honeycombs core layer on elastic foundations subjected to blast and damping loads. Int J Mech Sci 2017;133:504–12.
[75] Mahesh V. Nonlinear damping of auxetic sandwich plates with functionally graded magneto-electro-elastic facings under multiphysics loads and electromagnetic circuits. Compos Struct 2022;290:115523.
[76] Peng XL, Soyarslan C, Bargmann S. Phase contrast mediated switch of auxetic mechanism in composites of infilled re-entrant honeycomb microstructures. Extreme Mech Lett 2020;35.
[77] SeokLyoo W, ShikHa W. *In situ* fibrillation of poly(vinyl alcohol) during saponification of poly(vinyl ester) (1). Chemorheological and morphological investigations of *in situ* fibrillation. Polymer 1999;40(2) (Guildf).